

# First principles study of rare-earth oxides

L. Petit<sup>1,2</sup>, A. Svane<sup>2</sup>, Z. Szotek<sup>3</sup>, and W.M. Temmerman<sup>3</sup>

<sup>1</sup> *Computer Science and Mathematics Division,  
and Center for Computational  
Sciences, Oak Ridge National Laboratory,  
Oak Ridge, TN 37831, USA*

<sup>2</sup> *Department of Physics and Astronomy,  
University of Aarhus,  
DK-8000 Aarhus C, Denmark*

<sup>3</sup> *Daresbury Laboratory, Daresbury,  
Warrington WA4 4AD, UK*

(Dated: November 26, 2024)

## Abstract

The self-interaction-corrected local-spin-density approximation is used to describe the electronic structure of dioxides,  $\text{REO}_2$ , and sesquioxides,  $\text{RE}_2\text{O}_3$ , for the rare earths,  $\text{RE}=\text{Ce, Pr, Nd, Pm, Sm, Eu, Gd, Tb, Dy}$  and  $\text{Ho}$ . The valencies of the rare earth ions are determined from total energy minimization. We find Ce, Pr, Tb in their dioxides to have the tetravalent configuration, while for all the sesquioxides the trivalent groundstate configuration is found to be the most favourable. The calculated lattice constants for these valency configurations are in good agreement with experiment. Total energy considerations are exploited to show the link between oxidation and  $f$ -electron delocalization, and explain why, among the dioxides, only the  $\text{CeO}_2$ ,  $\text{PrO}_2$ , and  $\text{TbO}_2$  exist in nature. Tetravalent  $\text{NdO}_2$  is predicted to exist as a metastable phase - unstable towards the formation of hexagonal  $\text{Nd}_2\text{O}_3$ .

PACS numbers:

## I. INTRODUCTION

Even though the rare-earth (RE) elements readily oxidize, they do so with varying strength.<sup>1</sup> Ce metal oxidizes completely to CeO<sub>2</sub> in the presence of air. Pr occurs naturally as Pr<sub>6</sub>O<sub>11</sub>, exhibiting a slightly oxygen deficient fluorite structure. The stoichiometric fluorite structure PrO<sub>2</sub> exists under positive oxygen pressure. The rare-earth oxides from Nd onwards, with the exception of Tb, all occur naturally as sesquioxides, RE<sub>2</sub>O<sub>3</sub>. Tb oxide occurs naturally as Tb<sub>4</sub>O<sub>7</sub>, and transforms into TbO<sub>2</sub> under positive oxygen pressure.

The present study is concerned with the valencies of the oxides of Ce, Pr, Nd, Pm, Sm, Eu, Gd, Tb, Dy and Ho. Under suitable conditions, all the RE elements form a sesquioxide,<sup>2</sup> and there is general agreement that, in the corresponding groundstate, the rare-earth atoms are in the trivalent, RE<sup>3+</sup> configuration.<sup>3,4</sup> Each rare-earth atom donates 3 electrons to the strongly electronegative O ions, and the remaining 4*f* electrons stay strongly localized at the rare-earth site. In the lighter lanthanides, the *f*-electrons are less tightly bound, resulting in compounds that display a larger oxygen coordination number, CeO<sub>2</sub> and PrO<sub>2</sub>. Similarly in Tb, the extra electron on top of the half filled shell is less tightly bound resulting in a valency larger than 3+.

Only Ce, Pr, and Tb form dioxides, and with respect to the valency of the corresponding RE-ions the debate is still ongoing. Two conflicting points of view, both based on the interpretation of core-level spectroscopy studies, describe the dioxide groundstate as either tetravalent<sup>5,6,7</sup> or intermediate-valent.<sup>8,9,10</sup> The intermediate-valent interpretation uses the spectroscopic data to obtain the model parameters entering the Anderson impurity Hamiltonian.<sup>11</sup> By solving this many-body Hamiltonian<sup>12</sup> the initial state is derived from the final-state photoemission spectra. It should be noted however that Wuilloud *et al.*<sup>6</sup> derive the tetravalent groundstate for CeO<sub>2</sub>, using the same method. Marabelli and Wachter<sup>13,14</sup> conclude from their optical spectroscopy measurements that CeO<sub>2</sub> is a tetravalent insulator. Neutron scattering results on PrO<sub>2</sub>, by Kern *et al.*<sup>15</sup> were interpreted in terms of a localized 4*f*<sup>1</sup> groundstate configuration of the Pr ion. Similarly, recent neutron spectroscopy measurements of the magnetic excitations in PrO<sub>2</sub> have also been interpreted in terms of a tetravalent 4*f*<sup>1</sup> configuration.<sup>16</sup> With respect to the XPS results on PrO<sub>2</sub>, the proponents of the tetravalent picture explain the data in terms of the coexistence of localized and delocalized *f*-electrons.<sup>7</sup>

The rare-earth oxides find important applications in the catalysis, lighting and electronics industries and thus are extremely interesting compounds in their own right. A further reason for the strong interest in the RE-dioxides is their relation to the 123-cuprates  $\text{REBa}_2\text{Cu}_3\text{O}_7$ . One notices for example that it is again Ce, Pr and Tb that distinguish themselves from the other rare earth elements, as their corresponding cuprates do not support superconductivity.<sup>17</sup> Also in this case, no definite picture of the valency of the rare-earth ion has yet emerged. Similar to the intermediate-valency interpretation of the  $\text{PrO}_2$  data, it has been suggested that the suppression of superconductivity in  $\text{PrBa}_2\text{Cu}_3\text{O}_7$ , is associated with the existence of intermediate-valent Pr ions.<sup>18</sup> The determination of the valency configuration in the dioxides might thus be very useful for the elucidation of the mechanism behind superconductivity in the cuprates.

Any theoretical description of the rare-earth oxides needs to take into account the strong on-site  $f$ - $f$  interactions that push the  $4f$ -electrons towards localization. Using the Anderson impurity Hamiltonian, a possible approach is to derive the intraatomic Coulomb energy  $U$  from experiment, as was done in connection with the interpretation of XPS data.<sup>7</sup> There is also a possibility of obtaining the parameters of the Hamiltonian from first principles calculations, as was done by McMahan *et al.*<sup>19</sup> Electronic structure calculations, based on density functional theory have been very successful in describing the cohesive properties of solid-state systems with itinerant valence electrons. However the exchange and correlation effects of the homogeneous electron gas, which are included in the local-spin-density (LSD) approximation, are insufficient to account for the strong correlations experienced by the localized  $4f$ -electrons in the rare-earth compounds. With respect to the rare-earth oxides, the band structure calculations that we could find in literature are for  $\text{CeO}_2$ ,<sup>20,21,23</sup>  $\text{PrO}_2$ ,<sup>20,24</sup>  $\text{Ce}_2\text{O}_3$ ,<sup>21,23</sup>, and RE-sesquioxides in general.<sup>25</sup> From these studies it becomes clear that for example  $\text{CeO}_2$  is best described in terms of itinerant  $f$ -electrons, whilst for  $\text{Ce}_2\text{O}_3$ , considering one Ce  $f$ -electron as part of the core leads to better agreement with the experimental lattice parameter.<sup>21</sup> In this case, the  $f$ -electron groundstate configuration, and consequently the choice of calculational tool, is determined from a comparison to empirical data. Fabris *et al.*<sup>23</sup> show that the LDA+ $U$  approach gives good agreement with experiment for both Ce polymorphs, but the method requires input of a Hubbard  $U$  parameter (3 eV for Ce). In  $\text{PrO}_2$  the LSD description reveals a large  $f$ -peak at the Fermi level, in disagreement with the fact that  $\text{PrO}_2$  is an insulator.

In the self-interaction-corrected (SIC) local-spin-density approach<sup>26,27</sup> of the present paper, both localized and delocalized  $f$ -electrons are assumed to coexist. The delocalized  $f$ -levels move in the LSD potential, their exchange and correlation energies are those derived on the basis of the homogeneous electron gas, and their ability to form bands leads to a gain in hybridization energy. The localized  $f$ -levels acquire core-like character by correction of the LSD total energy functional for their spurious self-Coulomb and self-exchange-correlation energies.<sup>28</sup> This leads to an additional negative potential term and effectively prevents any hybridization. In the SIC-LSD approach, the localized and itinerant  $f$ -states are treated on an equal footing, and configurations with varying numbers of localized  $f$ -states can be compared with respect to their total energies. Consequently the preferred groundstate configuration, as far as the number of localized  $f$ -electrons is concerned, can be determined from the global total energy minimum. Namely by comparing the total energies resulting from different electronic configurations, one can determine whether it is favourable for the  $f$ -electrons to localize or to contribute to the band formation. The method has previously been successfully applied to describe the valencies of the RE elements<sup>29</sup> and compounds (see for example [30] and references therein).

The remainder of this paper is organized as follows. In section II and III respectively the results for the RE-dioxides and RE-sesquioxides are presented and compared to experiment. In section IV, the oxidation/reduction process is studied, and in section V, we draw our conclusions.

## II. THE RE-DIOXIDES

The SIC-LSD approach has been implemented using the tight-binding linear muffin-tin orbital (LMTO) method<sup>31</sup> in the atomic sphere approximation (ASA). The spin-orbit interaction is included in the Hamiltonian. Empty spheres are inserted on high symmetry interstitial sites. The valence panel includes the 6s, 5p, 5d and 4f orbitals on the rare-earth atom, and the 2s and 2p on the O atom, while the higher order  $\ell$  orbitals of O (3d and 4f), as well as all degrees of freedom of the empty spheres are treated as downfolded.<sup>31</sup> A separate energy panel is used to describe the semicore 5s states of the rare earth. In the valence band, we need to distinguish between those  $f$ -electrons that are SIC-localized, and the delocalized  $f$ -electrons, which together with the  $s$ ,  $p$  and  $d$  electrons constitute

Compound	$E_{IV} - E_{III}$	$V_{theo.}$	$V_{exp.}$
CeO <sub>2</sub>	-2.40	39.61	39.6
PrO <sub>2</sub>	-1.44	39.22	39.4
NdO <sub>2</sub>	-0.65	39.37	-
PmO <sub>2</sub>	-0.18	39.15	-
SmO <sub>2</sub>	0.49	42.19	-
EuO <sub>2</sub>	2.31	41.87	-
GdO <sub>2</sub>	1.22	41.08	-
TbO <sub>2</sub>	-0.27	36.50	35.6
DyO <sub>2</sub>	0.05	39.65	-
HoO <sub>2</sub>	0.46	39.06	-

TABLE I: Dioxide data: Column 2: Energy difference between tetravalent and trivalent configurations (in eV). Column 3: Theoretical volume in ( $\text{\AA}^3$ ). Column 4: Experimental volume in ( $\text{\AA}^3$ ) from Ref. 32.

the valence electrons. Different electronic configurations will give rise to different nominal valencies which in the SIC-LSD approach are defined as:  $N_{val} = Z - N_{core} - N_{SIC}$ , where  $Z$  is the atomic number,  $N_{core}$  is the number of atomic core and semicore electrons, and  $N_{SIC}$  is the number of localized  $f$  electrons. According to this definition, a localized  $f^1$  configuration of the RE ion will be referred to as trivalent in the case of Ce, tetravalent in the case of Pr, pentavalent in the case of Nd, etc..

The total energies of all the RE-dioxides from CeO<sub>2</sub> to HoO<sub>2</sub> were calculated with a rare earth valency assumed to be either 3, 4 or 5. In all these cases the crystal structure was taken to be the cubic fluorite structure. The results are listed in Table I, where the energy differences between the tetravalent and trivalent configuration,  $E_{IV} - E_{III}$ , are displayed in column 2. Here, a negative value indicates that the compound prefers the tetravalent groundstate configuration. The pentavalent configuration is found to be energetically unfavourable in all the dioxides. An example of the calculations involved in determining the energetically most favourable groundstate configuration is shown in Fig. 1 for PrO<sub>2</sub>. In this figure, the total energy of respectively pentavalent (Pr( $f^0$ )), tetravalent (Pr( $f^1$ )), and trivalent (Pr( $f^2$ )) PrO<sub>2</sub>, is plotted as a function of volume. The global energy minimum is

obtained in the tetravalent configuration. The theoretical equilibrium volume is calculated to be  $V_{tetv}=39.2 \text{ \AA}^3$ , which is in excellent agreement with the experimental value  $V_{exp}=39.4 \text{ \AA}^3$ .

A closer examination of the electronic structure reveals why the trivalent configuration is energetically unfavourable. In Fig. 2, both the total and  $f$ -projected DOS of  $\text{PrO}_2$  are shown for the pentavalent (Fig. 2a), tetravalent (Fig. 2b), and trivalent (Fig. 2c) Pr configurations. In Fig. 2a with all the  $f$ -electrons treated as delocalized, we find the Fermi level in the  $f$ -peak, in accordance with the LSD calculations by Koelling *et al.*,<sup>20</sup> and, as noted earlier, in disagreement with the observed insulating nature of  $\text{PrO}_2$ . Localizing one  $f$ -electron, results in the DOS of Fig. 2b, where now the Fermi level is situated inside the large gap, which forms between the occupied O  $p$  states and the unoccupied conduction bands of primarily Pr  $d$  character. Even though one  $f$ -electron has become localized, we still observe considerable  $f$  hybridization with the O  $p$ -band, i. e., the O  $p$ -states have large spatial extent and their tails reach into the atomic sphere around the RE atom, where they, when decomposed into RE-centred spherical harmonics, attain appreciable  $f$  character.

In this respect, both localized and delocalized  $f$ -electrons coexist in the tetravalent configuration, which is in line with the interpretation of X-ray absorption studies.<sup>6,7</sup> Finally, in the trivalent scenario of Fig. 2c, a further  $f$ -electron becomes localized, which results in the Fermi level moving down into the  $p$ -band. The O  $p$ -band states are depopulated to facilitate the formation of Pr  $f^2$  ions, i.e. charge transfer is imposed on the system, and the associated cost in energy is significantly larger than the gain in  $f$ -localization energy. The calculated energy minimum for the trivalent  $f^2$  configuration is situated more than 1 eV above the tetravalent energy minimum ( $E_{IV}-E_{III}=-1.44 \text{ eV}$ ), implying that localizing one more  $f$ -electron with respect to the tetravalent configuration results in a loss of hybridization and electrostatic energy ( $\sim 2.5 \text{ eV}$ ) that considerably exceeds the corresponding gain in SIC localization energy ( $\sim 0.95 \text{ eV}$  per  $f$ -electron). According to the proponents of the intermediate valency, the groundstate of  $\text{PrO}_2$  consists of a 50:50 mixture of  $4f^1$  and  $4f^2$  states,<sup>8,9,10</sup> with an average  $4f$  occupancy of approximately 1.5 electrons. In the present picture this would imply the trivalent and tetravalent configurations to be nearly energetically degenerate. This does not occur, as our total energy results point towards a relatively solid tetravalent groundstate configuration for  $\text{PrO}_2$ . The calculated band gap for  $\text{PrO}_2$  is approximately 1.1 eV, considerably larger than the 0.262 eV derived from conductivity

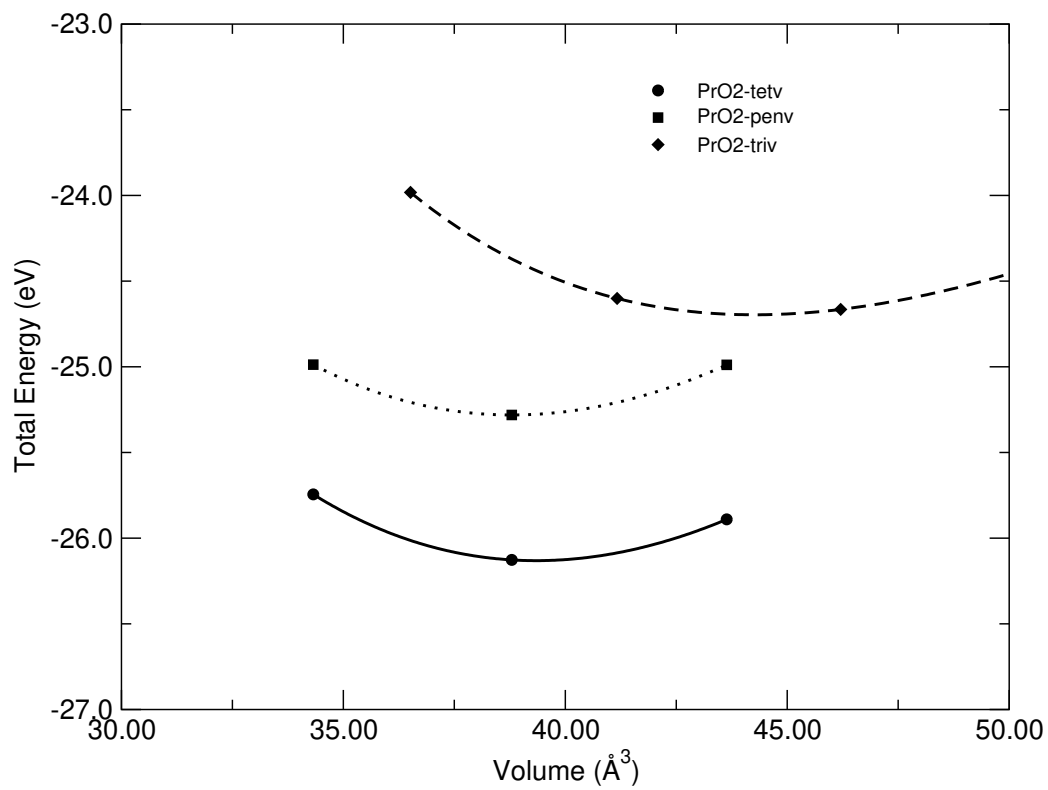


FIG. 1: Total energies (in eV per formula unit) as a function of volume (in  $\text{\AA}^3$ ) for  $\text{PrO}_2$ , assuming the Pr ions to be pentavalent ( $f^0$ , dotted line), tetravalent ( $f^1$ , solid line), and trivalent ( $f^2$ , dashed line), respectively. The global energy minimum is obtained in the tetravalent configuration.

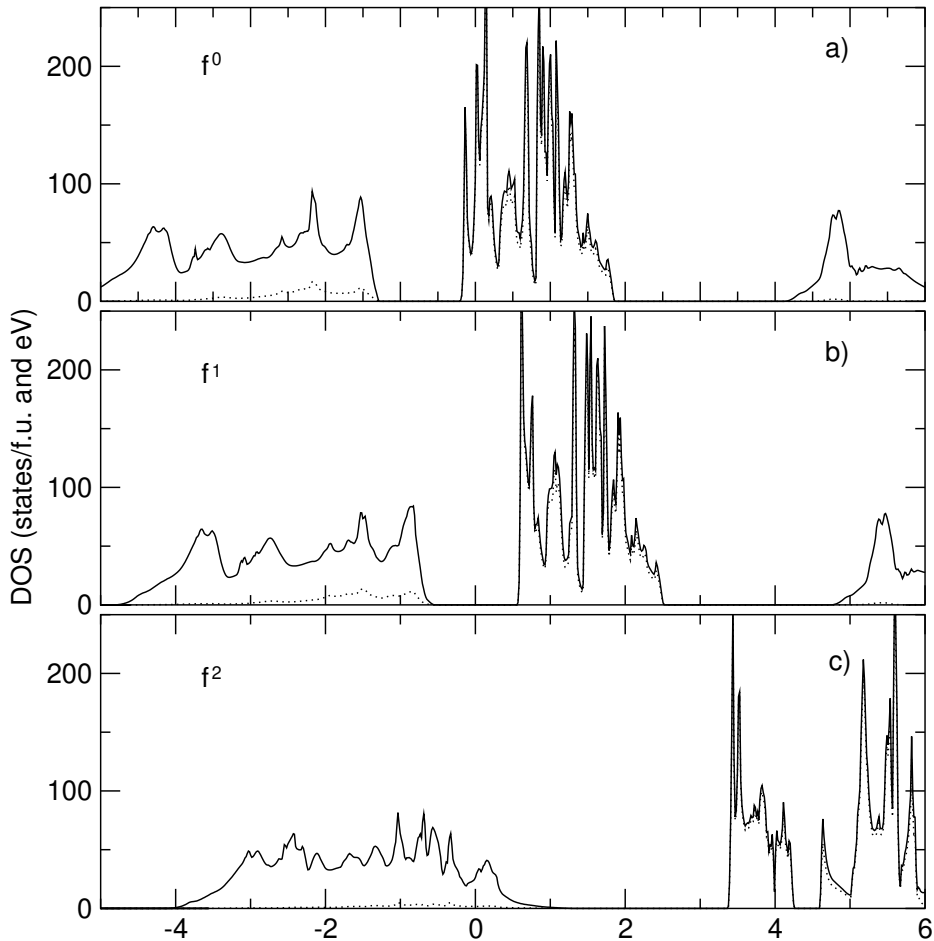


FIG. 2: Total DOS (solid line) and  $f$ -projected DOS (dotted line) for  $\text{PrO}_2$ , with the Pr ions in a) the pentavalent ( $f^0$ ) configuration b) the tetravalent ( $f^1$ ) configuration and c) the trivalent ( $f^2$ ) configuration. The energy is in units of eV, with zero marking the Fermi level.

measurements by Gardiner *et al.*<sup>33</sup>

For  $\text{CeO}_2$  we find a clearly preferred tetravalent groundstate configuration (the trend towards delocalization of the  $f$ -electrons is even stronger than in  $\text{PrO}_2$ ), i.e.  $\text{CeO}_2$  is best described in the LSD approximation, in line with results from earlier band structure calculations.<sup>20,21</sup> The calculated volume in this configuration is in good agreement with the experimental value, as can be seen from Table I.

In conclusion, our calculations do not confirm an intermediate-valent groundstate for either  $\text{PrO}_2$  and  $\text{CeO}_2$ . Koelling *et al.*<sup>20</sup> argued that, the intermediate valency scenario, is related to an ionic description of the RE-oxides, which can not account for the covalent  $f$ - $p$  bonding. In the ionic picture, valency is defined as the number of electrons that have been



transferred from the RE-atoms to the O-atoms, i.e.  $f$ -electrons do not participate in the bonding, and can only exist as localized at the RE-sites. A given configuration thus has an integral number of  $f$ -electrons, and a non-integral number of  $f$ -electrons can consequently only result from an intermediate-valency scenario. In the SIC picture both localized and delocalized  $f$ -states coexist. The delocalized  $f$ -electrons are allowed to participate in the band formation, and occur as part of the tails of O  $p$  states. The overall number of  $f$ -electrons is non-integral, in analogy to the intermediate valent ionic picture, but as a consequence of the  $p - f$  mixing.

Apart from Ce and Pr, Tb also forms a dioxide, albeit under positive oxygen pressure. We find the tetravalent groundstate configuration also to be energetically most favourable for TbO<sub>2</sub>, although here the energy difference, between the trivalent and tetravalent configurations is less pronounced than for PrO<sub>2</sub>. Again the volume, calculated for the tetravalent configuration is in good agreement with the experimental value. The remaining RE dioxides do not form in nature, and the determination of their groundstate configuration might seem of academic interest only. The energy differences,  $E_{IV} - E_{III}$ , in Table I, indicate that NdO<sub>2</sub>, and PmO<sub>2</sub> would also prefer the RE<sup>4+</sup> ion configuration. One notices however a decreasing affinity for the tetravalent configuration from CeO<sub>2</sub> to PmO<sub>2</sub>, and from SmO<sub>2</sub> the energy difference changes sign, indicating that now the trivalent configuration is energetically more favourable. With increasing nuclear charge, the  $f$ -electrons become more tightly bound to the RE atom, and the decreased overlap with neighbouring atoms results in a reduced gain in binding energy. Eventually it becomes more favourable to localize an extra electron, and gain the corresponding SIC energy, which is what happens in SmO<sub>2</sub>, with a resulting trivalent groundstate configuration. In the late RE dioxides, only TbO<sub>2</sub> is observed to be tetravalent, which is due to the fact that the Tb ion prefers a half-filled  $f$ -shell.

### III. THE RE-SESQUIOXIDES

Below 2000 C, the rare-earth sesquioxides adopt three different structure types.<sup>2</sup> The light RE crystallize in the hexagonal La<sub>2</sub>O<sub>3</sub> structure (A-type), and the heavy RE crystallize in the cubic Mn<sub>2</sub>O<sub>3</sub> structure (C-type), also known as the bixbyite structure. The middle RE can be found in either the C-type structure, or the B-type, which is a monoclinic distortion of the C-type structure. Conversions between the different structure types are induced under

Compound	$E_{IV} - E_{III}$ (eV)	$V_{hexag.}$ ( $\text{\AA}^3$ )		$V_{cubic}$ ( $\text{\AA}^3$ )	
	hexagonal	Theory	Expt.	Theory	Expt.
Ce <sub>2</sub> O <sub>3</sub>	0.38	76.4	79.4	87.27	87.0
Pr <sub>2</sub> O <sub>3</sub>	0.78	75.6	77.5	85.08	86.7
Nd <sub>2</sub> O <sub>3</sub>	0.94	74.0	76.0	83.52	85.0
Pm <sub>2</sub> O <sub>3</sub>	0.97	72.9	74.5	82.92	83.0
Sm <sub>2</sub> O <sub>3</sub>	1.09	72.0		81.27	81.7
Eu <sub>2</sub> O <sub>3</sub>	1.13	70.5		-	80.2
Gd <sub>2</sub> O <sub>3</sub>	1.29	68.8		79.43	79.0
Tb <sub>2</sub> O <sub>3</sub>	1.12	67.6		78.21	77.2
Dy <sub>2</sub> O <sub>3</sub>	1.21	66.3		77.78	75.9
Ho <sub>2</sub> O <sub>3</sub>	1.36	65.2		79.72	74.7

TABLE II: Sesquioxide data: Column 2: Energy difference between tetravalent and trivalent configurations (A-type structure). The experimental  $c/a$  ratio was used in the calculations. Columns 3 and 4: A-type theoretical and experimental volumes. Columns 5 and 6: C-type theoretical and experimental volumes. Experimental volumes are from [32].

specific temperature and pressure conditions.<sup>34</sup> We investigated the electronic structure of both the A-type and C-type sesquioxides. The C-type bixbyite structure was approximated by the fluorite REO<sub>2</sub> structure, with 1/4 of the O atoms removed.

Starting with the hexagonal A-type structure, we see from Table II, column 2, that all the sesquioxides prefer the trivalent groundstate configuration, in agreement with experiment. The degree of trivalency,  $E_{IV}-E_{III}$ , increases from Ce<sub>2</sub>O<sub>3</sub> to Gd<sub>2</sub>O<sub>3</sub>, then decreases slightly at Tb<sub>2</sub>O<sub>3</sub>, to increase again through Dy<sub>2</sub>O<sub>3</sub> to Ho<sub>2</sub>O<sub>3</sub>. Similar trends were obtained for the cubic C-type sesquioxides. The fact that the energy difference is less for Tb<sub>2</sub>O<sub>3</sub> than Gd<sub>2</sub>O<sub>3</sub>, indicates that the tetravalent half-filled  $f$ -shell configuration becomes relatively more important. For this same reason, trivalent Gd<sub>2</sub>O<sub>3</sub> is energetically very favourable.

Apart from the extraordinary stability of the half-filled shell configuration, the general tendency towards trivalency is clearly related to the increasing localization of the  $f$ -electrons with atomic number. The highly directional  $f$ -orbitals are only partially able to screen each other from the attractive force of the nucleus, which results in a steadily increasing effective

nuclear charge with increasing number of  $f$ -electrons. The increase in localization leads to the well known lanthanide contraction, i.e. the decrease in ionic radii across the rare earth series, which is also reflected in the lattice parameters of the sesquioxides. In Table II, the experimental and theoretical volumes are compared, for the A-type (columns 3 and 4) and C-type (columns 5 and 6) sesquioxides. The data are also illustrated in Fig. 3. Good agreement is seen with respect to both the overall trends and the absolute values. For the A-type hexagonal structures, the experimental  $c/a$  ratio was used, *i.e.*, no optimization of this parameter was attempted. From Fig. 3, we notice that the agreement between theory and experiment is considerably better for the C-type structure than for the A-type one. This might be related to the ASA used in the calculations. This geometrical approximation is likely less reliable when applied to the hexagonal A-structures, than when applied to the higher symmetry cubic C-structure. Figure 3 also includes the equilibrium volumes calculated by Hirosaki *et al.*<sup>25</sup>, using the projector augmented-wave (PAW) pseudopotential method, with the localized partly filled  $f$ -shell being treated as part of the core. For the A-type structure, the SIC-LSD calculations consistently yield lower volumes than observed, while the PAW values are consistently above. For the C-type structure, the present SIC-LSD calculations agree somewhat better with observations than the PAW results, in particular for the earlier REs, which may be due to the core approximation made for the  $f$ -electrons in the work of Ref. [25], and which may be too restrictive in the earlier RE sesquioxides.

The DOS and bandstructures for all the sesquioxides are quite similar and as a representative example in the Figs. 4 and 5 we present those of  $\text{Nd}_2\text{O}_3$ , as calculated in the trivalent ground state  $4f^3$  configuration. The broad band below the Fermi level originates from the  $O-p$  states. Hybridization and charge transfer result in this band being completely filled, leaving behind an empty  $f$ -peak situated in the gap between the valence and (non- $f$ )conduction bands. We find all the sesquioxides to be insulators.

In Table III, we compare the calculated band gaps for the A-type structure, to the experimental values, as obtained respectively from optical<sup>35</sup> (column 4) and conductivity<sup>36,37</sup> (columns 5 and 6) measurements. The two sets of conductivity measurements refer respectively to temperature regions above<sup>36</sup> (column 5) and below<sup>37</sup> (column 6)  $T=800$  K. We notice a considerable discrepancy between the optical and conductivity measurements, and the two sets of results have been interpreted slightly differently. In Fig. 6 we show schematically the various transitions that can be envisaged to occur. The actual transition

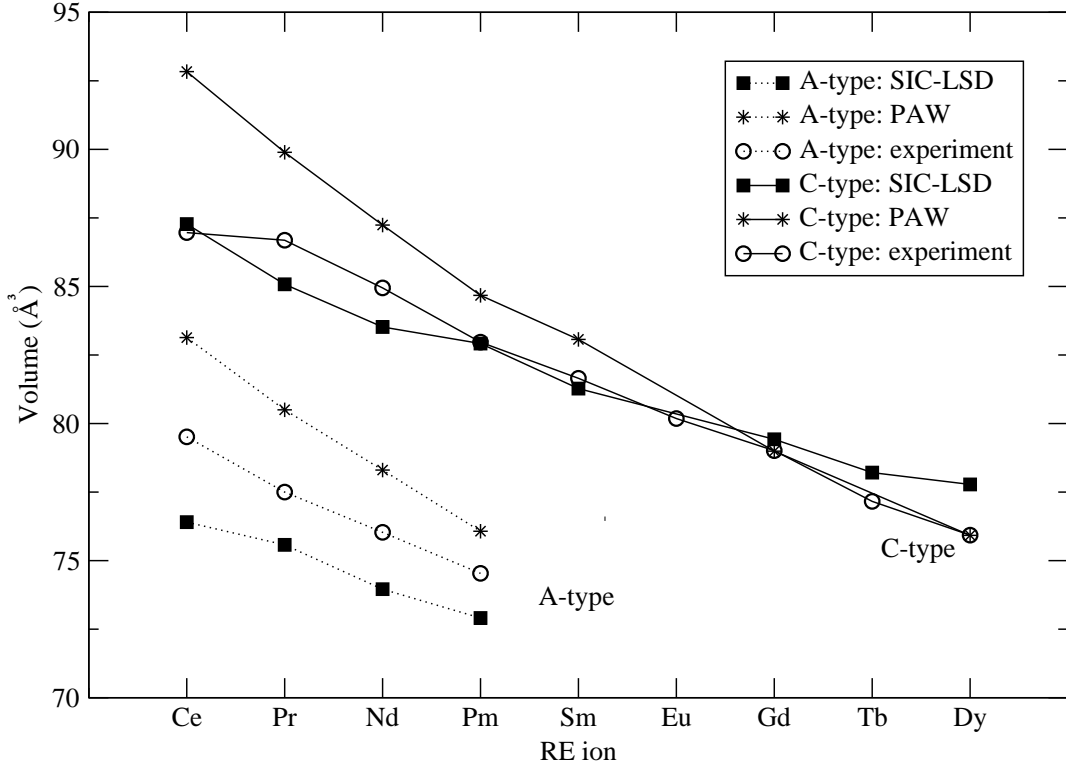


FIG. 3: Calculated equilibrium volumes of the rare-earth sesquioxides, crystallizing in the hexagonal A-type structure (dotted line), and the cubic C-type structure (full line). The stars, circles, and squares refer to the PAW,<sup>25</sup> SIC-LSD (present), and experimental results.<sup>32</sup>

depends crucially on the position of the occupied and empty  $f$ -states, respectively  $f^n$  and  $f^{n+1}$ . The interpretation of the optical data is that the empty  $f$ -levels are situated above the conduction band minimum (CBM), and the energy gap  $E_g$  is entirely determined by the gap between the occupied  $f$ - and the CBM. If the  $f$ -states move below the valence band maximum (VBM), the band gap becomes largest (i.e.  $v \rightarrow c$ ). The activation energies  $E_a$  in column 5, obtained from conductivity measurements (using  $\text{conductivity} \sim e^{-E_a/2kT}$ ) indicate that, for some compounds, the transition is from ( $v \rightarrow f$ ), i.e. that the empty levels can be situated in the gap between VBM and CBM.

One could speculate whether the absence of ( $v \rightarrow f$ ) transitions in the optical spectrum is due to this transition being optically forbidden, whilst no such constraint exists for the thermal excitations, which go into the unoccupied  $f$ -bands. However this can not explain the relatively large difference in the gap energy, observed for example in the case of  $\text{Gd}_2\text{O}_3$ , where both optical and conductivity measurements agree on the nature of the gap being

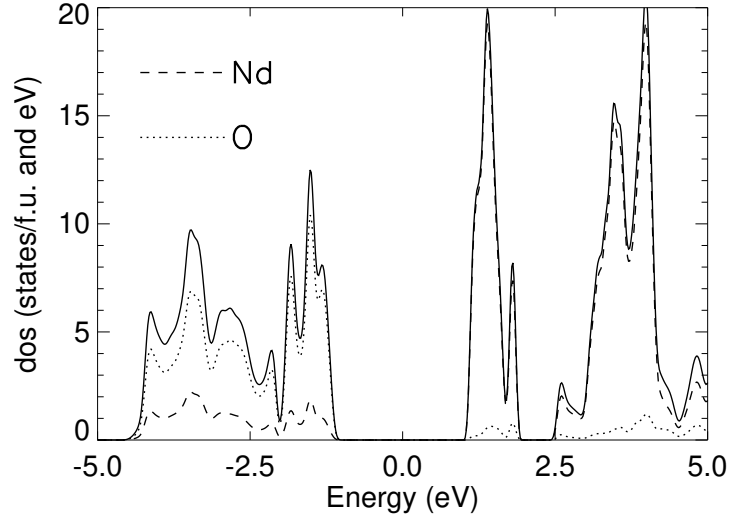


FIG. 4: Total DOS of  $\text{Nd}_2\text{O}_3$  in the trivalent ( $f^3$ ) configuration in the A-type hexagonal structure at the calculated equilibrium volume. Energy is in eV, with 0 marking the mid-gap position, while DOS is in states per formula units and eV.

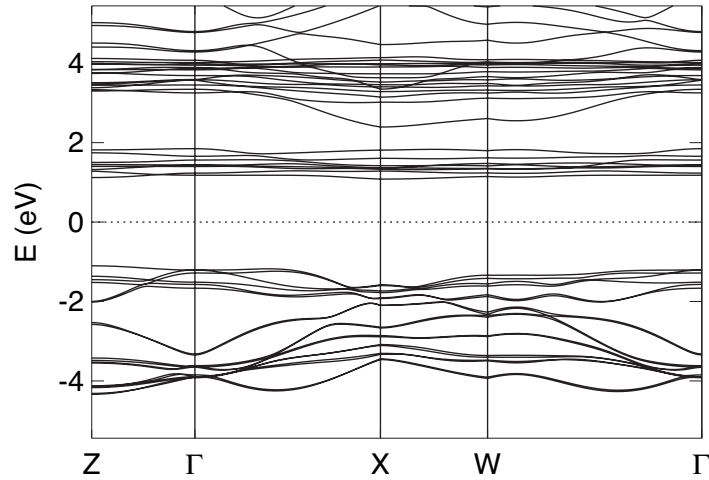


FIG. 5: Bandstructure of A-type  $\text{Nd}_2\text{O}_3$  in the trivalent configuration.

( $v \rightarrow c$ ). From the theoretical data we see that the gap between valence and conduction bands ( $v \rightarrow c$ ) shows a rather slow increase across the RE series, whereas the gap between valence and  $f$ -band ( $v \rightarrow f$ ) decreases from  $\text{Ce}_2\text{O}_3$  to  $\text{Eu}_2\text{O}_3$ , and from  $\text{Gd}_2\text{O}_3$  to  $\text{Dy}_2\text{O}_3$ . For  $\text{Ce}_2\text{O}_3$ ,  $\text{Pr}_2\text{O}_3$  and  $\text{Gd}_2\text{O}_3$  no separate edge for the non- $f$  conduction bands was found in the calculations. The direct comparison between calculated and experimental gaps is tricky. The

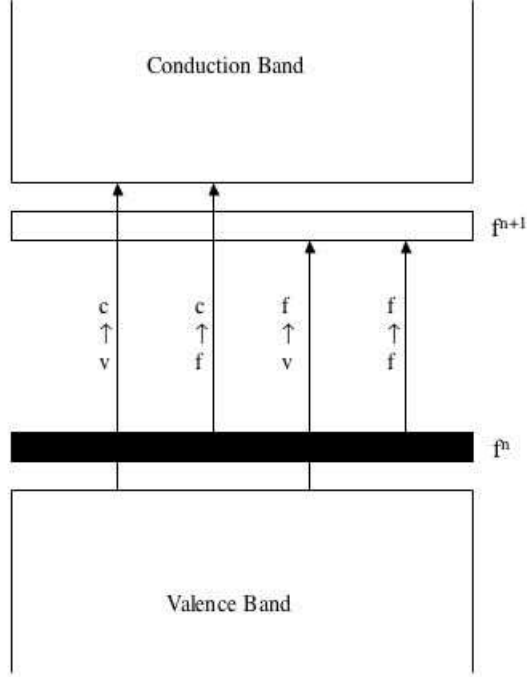


FIG. 6: Schematic representation of the RE sesquioxide band gap. The  $f^n$  and  $f^{n+1}$  depict respectively the occupied and empty  $f$ -bands.

SIC-LSD approach cannot accurately determine the removal energies of localized states, and the bare  $f$ -bands always appear at too high binding energies due to the neglect of screening and relaxation effects.<sup>38</sup> With the SI corrected  $f$ -states situated below the valence band edge, the calculated band-gaps are of either  $v$ - $f$  or  $v$ - $c$  character. The observed trend can be explained by the fact that with increasing atomic number the  $f$ -orbitals become increasingly localized, and the energy of the  $f$ -shell decreases. At  $\text{Gd}_2\text{O}_3$  all seven majority spins are SI-corrected, and the minority states are situated above the conduction band minimum. The  $v \rightarrow f$  gap starts decreasing again from  $\text{Tb}_2\text{O}_3$  as the minority states are pulled into the gap between valence and conduction band.

Our calculated values for  $v \rightarrow c$  are consistently smaller than the optical  $E_g$ . If the optical  $E_g$ 's turn out to be a better representation of the actual band gaps, the reason for the difference with our calculated results could be twofold: The LSD is known to underestimate

Compound	$E_{gap}$ (eV)				
	Theory		Experiment		
	$v \rightarrow f$	$v \rightarrow c$	optical $\sigma$	$\sigma$ (T=800-1200 K)	$\sigma$ (T< 800 K)
Ce <sub>2</sub> O <sub>3</sub>	3.20	3.20	2.4	-	-
Pr <sub>2</sub> O <sub>3</sub>	2.62	2.62	4.6	-	0.8 <sup>C</sup>
Nd <sub>2</sub> O <sub>3</sub>	2.13	3.58	4.4	2.36 <sup>A</sup> ( $f \rightarrow c$ )	-
Pm <sub>2</sub> O <sub>3</sub>	1.66	3.77	-	-	-
Sm <sub>2</sub> O <sub>3</sub>	1.04	3.80	5.0	2.12 <sup>B</sup> ( $v \rightarrow f$ )	1.2 <sup>C</sup>
Eu <sub>2</sub> O <sub>3</sub>	0.63	3.95	4.4	1.84 <sup>C</sup> ( $v \rightarrow f$ )	1.2 <sup>C</sup>
Gd <sub>2</sub> O <sub>3</sub>	3.13	3.13	5.3	2.64 <sup>C</sup> ( $v \rightarrow c$ )	1.0 <sup>C</sup>
Tb <sub>2</sub> O <sub>3</sub>	2.27	4.32	4.1	2.24 <sup>B</sup> ( $f \rightarrow c$ )	0.8 <sup>C</sup>
Dy <sub>2</sub> O <sub>3</sub>	1.71	4.39	4.9	2.82 <sup>C</sup> ( $v \rightarrow c$ )	-
Ho <sub>2</sub> O <sub>3</sub>	1.26	4.48	5.2	2.74 <sup>C</sup> ( $v \rightarrow c$ )	1.4 <sup>C</sup>

TABLE III: Sesquioxide band-gaps. Theoretical values for A-type structure: valence to  $f$ -band (column 2), valence to conduction band (column 3). Experimental values: optical measurements (column 4), columns 5 and 6 from conductivity measurements above and below 800 K respectively.

gaps between occupied and unoccupied bands, and in addition, the unoccupied  $f$  bands may be positioned extraordinarily low due to the neglect of correlation effects beyond the LSD for these. In order to discuss in more detail the accuracy of the calculated energy gaps, one would need to further investigate the reason behind the considerable discrepancy between the optical and conductivity measurements.

#### IV. OXIDATION

So far, the present theory has demonstrated that all the sesquioxides prefer the trivalent groundstate configuration, whilst the dioxides can be separated into tetravalent light RE-dioxides, and trivalent heavy RE-dioxides, with the exception of TbO<sub>2</sub>, which also prefers the tetravalent groundstate. From experiment however we know that all the RE-sesquioxides are found in nature, whilst the only dioxides that occur naturally are CeO<sub>2</sub>, PrO<sub>2</sub> and TbO<sub>2</sub>. With respect to the valencies, these two sets of information lead us to conclude that the

RE-sesquioxides are trivalent, and the naturally occurring RE-dioxides are tetravalent, *i. e.*, the oxidation process from sesquioxide to dioxide goes hand in hand with the delocalization of an extra  $f$ -electron. The extraordinary catalytic properties of Ceria are according to Skorodumova *et al.*<sup>39</sup> based on the coupling between  $f$ -electron localization and oxidation. Recent calculations<sup>40</sup> have similarly shown that, the possible existence of the higher oxidation state,  $\text{PuO}_{2+x}$ ,<sup>41</sup> can be explained by the occurrence of a Pu pentavalent state, which is reduced to a tetravalent state in  $\text{PuO}_2$ . The question remains however, why the dioxide only exists for Ce, Pr, and Tb. For example, from the data in Table I it follows that Nd in  $\text{NdO}_2$  also readily takes the tetravalent configuration, but nevertheless this compound does not occur naturally.

To discuss this issue, we consider the oxidation process:



The balance of this reaction in general will depend on the Gibb's free energy of the reactants at the given temperature and pressure. The ab-initio calculations of these quantities are beyond the capability of the present theory. However we can still to some extent analyze the reaction (1) by looking at the zero temperature and zero pressure limit. In that case the free energy difference between the reactants reduces to the corresponding total energy difference, as obtained by the SIC calculations:

$$E_{ox} \equiv 2E^{SIC}(\text{REO}_2) - E^{SIC}(\text{RE}_2\text{O}_3) - \mu_O. \quad (2)$$

Still, the comparison of the dioxide and sesquioxide total energies is not straightforward due to the approximations of the present SIC-LSD implementation, most notably the ASA. The total energies depend on the ASA radii chosen for the constituent atoms. The problem is most severe for the low symmetry hexagonal structure of the sesquioxides, and is the most probable reason why the calculated equilibrium volumes of the hexagonal sesquioxides are in somewhat poorer agreement with experiment, cf. Table II. Unfortunately, the SIC-LSD approach has only been implemented within the tight-binding LMTO-ASA method and not in its full potential version FP-LMTO, where the problems associated with the ASA would not occur. However, in the  $f^0$  groundstate configuration, the relative error introduced by the ASA, can be estimated from a comparison of the total energies, as obtained respectively with a FP-LMTO method and our LMTO-ASA implementation of the SIC-LSD method. This



$\text{REO}_2/\text{RE}_2\text{O}_3$	$E_{ox}(\text{A-RE}_2\text{O}_3)$	$E_{ox}(\text{C-RE}_2\text{O}_3)$
$\text{CeO}_2/\text{Ce}_2\text{O}_3$	<b>-1.90</b>	-3.54
$\text{PrO}_2/\text{Pr}_2\text{O}_3$	<b>-0.14</b>	-1.90
$\text{NdO}_2/\text{Nd}_2\text{O}_3$	<b>0.54</b>	-0.54
$\text{PmO}_2/\text{Pm}_2\text{O}_3$	0.00	<b>0.27</b>
$\text{SmO}_2/\text{Sm}_2\text{O}_3$	-0.82	<b>0.68</b>
$\text{GdO}_2/\text{Gd}_2\text{O}_3$	-10.88	<b>0.14</b>
$\text{TbO}_2/\text{Tb}_2\text{O}_3$	-8.16	<b>-0.27</b>
$\text{DyO}_2/\text{Dy}_2\text{O}_3$	-4.08	<b>0.27</b>
$\text{HoO}_2/\text{Ho}_2\text{O}_3$	-0.68	<b>0.00</b>

TABLE IV: Oxidation energies in eV (from equation (2)). Column 2: assuming the oxidation process involves the A-type sesquioxide, Column 3: assuming the oxidation process involves the C-type sesquioxide. Negative/positive energies indicate that the dioxide/sesquioxide is energetically most favourable. The bold characters indicate which type of sesquioxide will preferentially be formed, if at all.

provides a FP-ASA total energy correction, which can be used to calibrate the corresponding energies calculated with the SIC-LSD. Since the energy differences between the valency configurations of a given compound are almost unaffected by the chosen ASA radii, for a given compound the same correction can be applied to the total energies in the different localization configurations.

In the following, we assume that the dioxides and the C-type sesquioxides, which both crystallize in a cubic structure, are adequately described within the ASA approximation. The FP-ASA correction is therefore only applied to the A-type sesquioxide, which crystallizes in the hexagonal structure. In Table IV the resulting oxidation energies (2) assuming either the A or C-type sesquioxides are given in columns 2 and 3 respectively. The chemical potential used, is  $\mu_O = -6.12$  eV (relative to free atoms). A negative/positive energy balance means that the formation of the dioxide/sesquioxide is energetically most favourable. From the table we see that in the case of Ce, Pr, and Tb, the dioxide is preferred energetically with respect to both the A- and C-type sesquioxide. We also find that for Ce and Pr the A-type sesquioxide is least unfavourable with respect to the dioxide (as indicated by the relatively

smaller oxidation energy), whilst for Tb it is the C-type sesquioxide that is closest in energy to the dioxide. This is relevant since it indicates which sesquioxide structure will form in the reduction process. For Nd, we find the dioxide to be more favourable than the C-type sesquioxide, but less favourable than the A-type sesquioxide, i.e. at  $T=0$ , Nd exists as A-type  $\text{Nd}_2\text{O}_3$ .  $\text{NdO}_2$  may exist as a metastable phase, since steric effects may hinder the reduction of this compound into the hexagonal sesquioxide. As discussed, up to now the synthesis of  $\text{NdO}_2$  has not been successful. For the remaining RE, the C-type sesquioxide is more stable than the dioxide, as indicated by the positive oxidation energies. The relevant oxidation energies (indicated by boldface in Table IV) are plotted in Fig. 7 as a function of rare earth ion. The overall picture is that Ce, Pr, and Tb exist as dioxides, whilst the remaining RE prefer the sesquioxide, in agreement with experiment. It also shows that with respect to the sesquioxides, the later RE from Pm onwards crystallize in the C-type structure, whilst reduction of the early  $\text{REO}_2$  will result in sesquioxide crystallizing in the A-type, which again would be in good agreement with experiment.

There is some uncertainty in our results associated with the value of the oxygen chemical potential. We have conveniently used a value of  $\mu_{\text{O}} = -6.12$  eV, as it allows us to indicate the trend in oxidation energies more clearly. Actually, using a FP-LMTO calculation, with the  $\text{O}_2$  molecule put into a lattice with large lattice constant, we find  $\mu_{\text{O}} = -4.76$  eV, i.e. 1.36 eV less than the value used in Table IV. Using this value in Fig. 7 gives a qualitatively slightly different picture, as the oxide/sesquioxide borderline is now situated 1.36 eV higher (solid line), which means that in this scenario, the dioxide is always preferred. Again other LSD total energy calculations give a binding energy of 7.48 eV for the  $\text{O}_2$  molecule, and the experimental value is 5.17 eV.<sup>22</sup> We should also notice here, that the calculated total energies apply to  $T = 0$ , and under actual conditions, the reduction (left side of equation (1)) will be favoured by the higher entropy, as it leads to release of  $\text{O}_2$ . Higher temperature thus will work in favour of sesquioxide formation. It seems that the existence of tetravalent  $\text{CeO}_2$ ,  $\text{PrO}_2$  and  $\text{TbO}_2$  is an indication that their sesquioxides will readily oxidize. Conversely, we could interpret the trivalent configuration of the other RE-dioxides as evidence that their sesquioxides will not further oxidize.

## V. CONCLUSION

In conclusion, we used the SIC-LSD method to analyze the valencies of the rare-earth dioxides and sesquioxides. We find from total energy considerations, that  $\text{CeO}_2$ ,  $\text{PrO}_2$ , and  $\text{TbO}_2$  prefer the tetravalent configuration, with respectively zero, one, and seven localized  $f$ -electrons. The intermediate valency scenario is not found to be energetically viable, but non-integral total  $f$ -occupancies do occur due to covalent  $p - f$  mixing. The sesquioxides are all found to prefer the trivalent configuration, leading to insulating groundstates in agreement with experiment. The calculated equilibrium volumes for both the dioxides and the sesquioxides are in good agreement with the experimental values. The oxidation reaction from sesquioxide to dioxide is found to be accompanied by  $f$ -electron delocalization, and consequently only occurs for the early lanthanides and Tb, for which the  $f$ -electrons are least tightly bound.

### Acknowledgments

This work has been partially funded by the Training and Mobility Network on 'Electronic Structure Calculation of Materials Properties and Processes for Industry and Basic Sciences' (contract:FMRX-CT98-0178) and by the Research Training Network on 'Ab-initio Computation of Electronic Properties of f-electron Materials' (contract:HPRN-CT-2002-00295). Work of L.P. was sponsored in part by the Office of Basic Energy Sciences, U.S. Department of Energy. The Oak Ridge National Laboratory is managed by UT-Battelle LLC for the Department of Energy under Contract No. DE-AC05-00OR22725.

- 
- <sup>1</sup> E. Holland-Moritz, *Z. Phys. B* **89**, 285 (1992).
  - <sup>2</sup> L. Eyring, in *Handbook on the Physics and Chemistry of Rare Earths*, Vol. 3, edited by K. A. Gschneider Jr., and L. Eyring (North-Holland, Amsterdam, 1979), p. 337.
  - <sup>3</sup> S. Tanaka, H. Ogasawara, K. Okada and A. Kotani, *J. Phys. Soc. Jpn.* **64**, 2225 (1995).
  - <sup>4</sup> A. Moewes, D. L. Ederer, M. M. Grush and T. A. Callcott, *Phys. Rev. B* **59**, 5452 (1999).
  - <sup>5</sup> T. Hanyu, H. Ishii, M. Yanagihara, T. Kamada, T. Miyahara, H. Kato, K. Naito, S. Suzuki, and T. Ishii, *Solid State Commun.* **56**, 381 (1985).

- <sup>6</sup> E. Wuilloud, B. Delley, W.-D. Schneider and Y. Baer, Phys. Rev. Lett. **53**, 202 (1984).
- <sup>7</sup> R. C. Karnatak, J.-M. Esteve, H. Dexpert, M. Gasgnier, P. E. Caro and L. Albert, Phys. Rev. B **36**, 1745 (1987); H. Dexpert, R. C. Karnatak, J.-M. Esteve, J. P. Connerade, M. Gasgnier, P. E. Caro and L. Albert, Phys. Rev. B **36**, 1750 (1987).
- <sup>8</sup> A. Bianconi, A. Kotani, K. Okada, R. Giorgi, A. Gargano, A. Marcelli and T. Miyahara, Phys. Rev. B **38**, 3433 (1988).
- <sup>9</sup> H. Ogasawara, A. Kotani, K. Okada and B. T. Thole, Phys. Rev. B **43**, 854 (1991).
- <sup>10</sup> S. M. Butorin, L.-C. Duda, J.-H. Guo, N. Wassdahl, J. Nordgren, M. Nakazawa and A. Kotan, J. Phys. Condens. Matter **9**, 8155 (1997).
- <sup>11</sup> P. W. Anderson, Phys. Rev. B **24**, 41 (1961).
- <sup>12</sup> O. Gunnarsson and K. Schönhammer, Phys. Rev. B **28**, 4315 (1983).
- <sup>13</sup> F. Marabelli and P. Wachter, Phys. Rev. B **36**, 1238 (1987).
- <sup>14</sup> P. Wachter, Physica B **300**, 105 (2001).
- <sup>15</sup> S. Kern, C.-K. Loong, J. Faber Jr., and G. H. Lander, Solid State Commun. **49**, 295 (1984).
- <sup>16</sup> A. T. Boothroyd, C. H. Gardiner, S. J. S. Lister, P. Santini, B. D. Rainford, L. D. Noailles, D. B. Currie, R. S. Eccleston, and R. I. Bewley, Phys. Rev. Lett. **86**, 2082 (2001).
- <sup>17</sup> G. D. Chryssikos, E. I. Kamitsos, J. A. Kapoutsis, A. P. Patsis, V. Psycharis, A. Koufoudakis, Ch. Mitros, G. Kallias, E. Gamari-Seale, and D. Niarchos, Physica C **254**, 44 (1995).
- <sup>18</sup> R. Fehrenbacher and T. M. Rice, Phys. Rev. Lett. **70**, 3471 (1993).
- <sup>19</sup> A. K. McMahan and R. M. Martin, in *Narrow-Band Phenomena - Influence of Electrons with Both Band and Localized Character*, edited by J. C. Fuggle, G. A. Sawatzky, and J. W. Allen (Plenum, New York), p. 133.
- <sup>20</sup> D. D. Koelling, A. M. Boring, and J. H. Wood, Solid State Commun. **47**, 227 (1983).
- <sup>21</sup> N. V. Skorodumova, R. Ahuja, S. I. Simak, I. A. Abrikosov, B. Johansson, and B. I. Lundqvist, Phys. Rev. B **64**, 115108 (2001).
- <sup>22</sup> R. O. Jones and O. Gunnarsson, Rev. Mod. Phys. **61**, 689 (1989).
- <sup>23</sup> S. Fabris, S. de Gironcoli and S. Baroni, cond-mat/0312601 (2003).
- <sup>24</sup> H. Dabrowski, V. Zavodinski, and A. Fleszar, Microelectronics Reliability **41**, 1093 (2001).
- <sup>25</sup> N. Hirosaki, S. Ogata, and C. Kocer, J. Alloys Comp. **351**, 31 (2003).
- <sup>26</sup> W.M. Temmerman, A. Svane, Z. Szotek and H. Winter, in "Electronic Density Functional Theory: Recent Progress and New Directions" Eds J. F. Dobson, G. Vignale and M. P. Das, Plenum,

- NY (1998).
- <sup>27</sup> W.M. Temmerman, A.Svane, Z. Szotek, H. Winter and S. Beiden, in ”, Lecture Notes in Physics 535: ”Electronic structure and Physical Properties of Solids: The uses of the LMTO method”, ed. H. Dreyss, Springer-Verlag,286-312 (2000).
- <sup>28</sup> J. P. Perdew, and A. Zunger, Phys. Rev. B **23**, 5048 (1981).
- <sup>29</sup> P. Strange, A. Svane, W. M. Temmerman, Z. Szotek, and H. Winter, Nature (London) **399**, 756 (1999);
- <sup>30</sup> A. Svane, G. Santi, Z. Szotek, W. M. Temmerman, P. Strange, M. Horne, G. Vaitheeswaran, V. Kanchana, L. Petit, and H. Winter, phys. stat. sol. (b) **241**, 3185 (2004); G. Vaitheeswaran, L. Petit, A. Svane, V. Kanchana, and M. Rajagopalan, J. Phys. Condens. Matter **16**, 4429 (2004).
- <sup>31</sup> O. K. Andersen, O. Jepsen, and D. Glötzel, in *Canonical Description of the Band Structures of Metals*, Proceedings of the International School of Physics, ”Enrico Fermi”, Course LXXXIX, Varenna, 1985, eds. F. Bassani, F. Fumi, and M. P. Tosi, (North-Holland, Amsterdam, 1985).
- <sup>32</sup> P. Villars and L. D. Calvert, *Pearson’s Handbook of Crystallographic Data for Intermetallic Phases*, 2. ed., (ASM International, Ohio, 1991).
- <sup>33</sup> c. H. Gardiner, A. T. Boothroyd, P. Pattison, M. J. McKelvy, G. J. McIntyre, and S. J. S. Lister, Phys. Rev. B **70**, 024415 (2004).
- <sup>34</sup> H. R. Hoekstra and K. A. Gingerich, Science **146**, 1163 (1964).
- <sup>35</sup> A. V. Prokofiev, A. I. Shelykh, and B. T. Melekh, J. Alloys Comp. **242**, 41 (1996).
- <sup>36</sup> H. B. Lal, Gaur Kanchan, J. Mater. Sci. **23**, 919 (1988).
- <sup>37</sup> G. V. Subba Rao, S. Ramdas, P. N. Mehrotra, and C. N. R. Rao, J. Solid State Chem. **2**, 377 (1970).
- <sup>38</sup> W. M. Temmerman, Z. Szotek, and H. Winter, Phys. Rev. B **47**, 1184 (1993).
- <sup>39</sup> N. V. Skorodumova, S. I. Simak, B. I. Lundqvist, I. A. Abrikosov, and B. Johansson, Phys. Rev. Lett. **89**, 166601 (2002).
- <sup>40</sup> L. Petit, A. Svane, Z. Szotek and W.M. Temmerman, Science **301**, 498 (2003).
- <sup>41</sup> J.M. Haschke, T.H. Allen and L.A. Morales, Science **287**, 285 (2000).

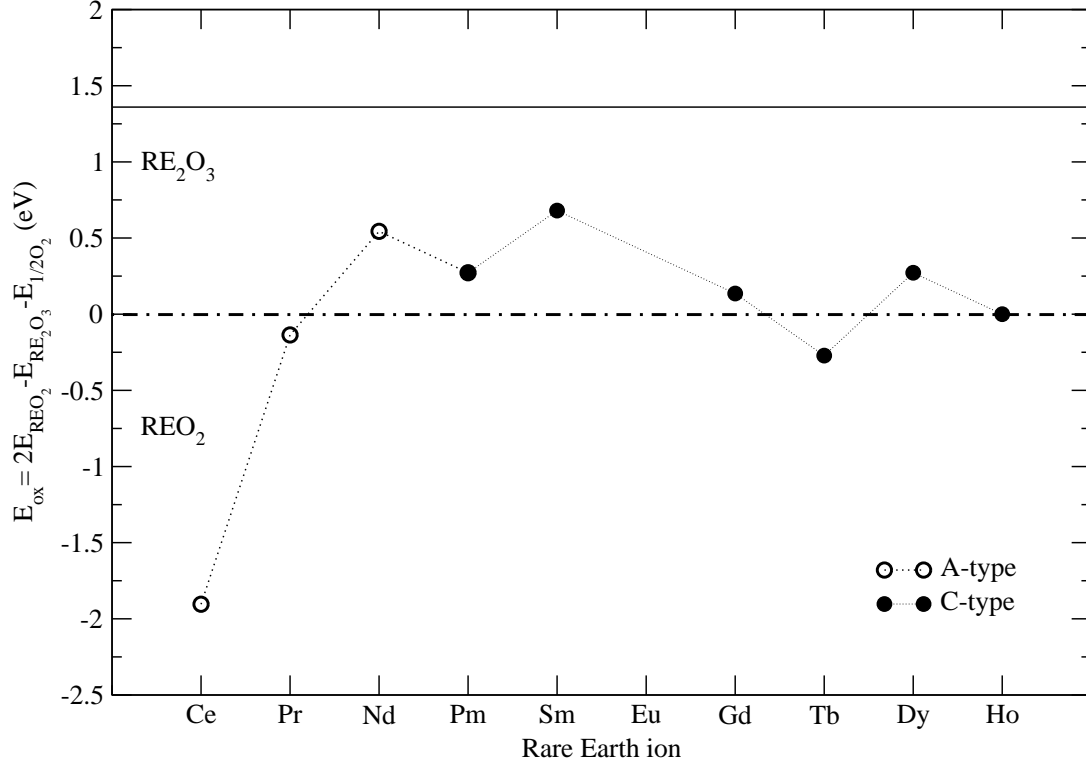


FIG. 7: Oxidation energies,  $E_{ox}$  in Eq. (2), for the rare earths Ce to Ho. The full circle is for the cubic C-type sesquioxide, the empty circle for the A-type hexagonal structure of the sesquioxide. Negative values indicate that the dioxide is stable. The chemical potential of free O is taken as  $\mu_O = -6.12$  eV. The solid line just below 1.5 eV indicates the dioxide/sesquioxide borderline in case the FP-LMTO calculated value  $\mu_O = -4.76$  eV is used.